NANO LETTERS

2007
Vol. 7, No. 10
3182−3188

A Gradient Microarray Electronic Nose Based on Percolating SnO_2 Nanowire Sensing Elements

Victor V. Sysoev,*,† Joachim Goschnick,*,‡ Thomas Schneider,‡ Evghenii Strelcov,§ and Andrei Kolmakov*,§

Department of Physics, Saratov State Technical University, Saratov 410054, Russia, Forschungszentrum Karlsruhe, Hermann-von-Helmholtz-Platz 1, Karlsruhe 76021, Germany, and Southern Illinois University, Carbondale, Illinois 62901-4401

Received July 25, 2007; Revised Manuscript Received September 3, 2007

ABSTRACT

Fabrication, characterization, and tests of the practical gradient microarray electronic nose with SnO_2 nanowire gas-sensing elements are reported. This novel device has demonstrated an excellent performance as a gas sensor and e-nose system capable of promptly detecting and reliably discriminating between several reducing gases in air at a ppb level of concentration. It has been found that, in addition to the temperature gradient across the nanowire layer, the density and morphological inhomogeneities of nanowire mats define the discriminating power of the electronic nose.

A key requirement in the development of gas-analytical sensor systems for industrial, medical, security, and even domestic applications is their ability to promptly and reliably "detect" and "recognize" a broad range of gases, often in low concentrations,[1] while working in a continuous mode. It is well-known that materials or chemical processes release characteristic complex gas ensembles (called odors if perceptible by the human nose) that can be used like a fingerprint for condition monitoring, an indispensable task of future intelligent systems and therefore an urgently needed key technology for tomorrow. A biology inspired but challenging approach to design appropriate sensor systems mimics the data acquisition principles of mammalian olfactory systems,[2,3] which allows one to discriminate single gases as well as odorlike gas ensembles by creating and processing a multidimensional pattern of many signals generated by a receptor (sensor) array.[4−7] Devices employing this pattern recognition concept are frequently called "electronic noses" (see terms, history, and references in the comprehensive monograph ref 8).

Recent developments in micro- and nanotechnologies[9−30] have made available new material platforms, device fabrication alternatives, and novel sensing concepts to improve sensitivity, reliability, energy consumption, and response time of the next generation sensors.

In particular, the recently fabricated quasi-one-dimensional (1D) metal oxide nanostructures[14−16] have been found to be outstanding for these applications because a multitude of sensing properties are substantially improved compared to compact metal oxide gas detecting elements. Namely, high surface-to-bulk ratio allows very sensitive transduction of the gas/surface interactions (adsorption or catalytic oxidation) into a change of the electrical conductivity.[17−25] The radius of these nanostructures approaches the material's Debye length, which makes nearly the whole nanowire a depletion (accumulation) zone of mobile charge carriers in response to surface redox process[26] and thus establishes an extreme sensitivity of the electron (hole) transport to charge transfer interactions of gas molecules at the surface. In addition, their ability to accept a variety of morphologies[14,27,28] and structures in conjunction with their surface and bulk doping[29] offers wide possibilities to tune the gas-sensing properties.[30,31] An advantage over nanostructured oxide films, which hamper the gas diffusion with reduction of the grain size, the nanowire layers render the empty space between the nanofibers no matter how small the diameter of the individual nanowires is. As a result, these structures are currently considered to be a prospective platform for the next generation of electronic (nano)-noses.[30]

However, despite encouraging demonstrations of an array of individual metal oxide nanowires,[32] there still exists a *technological gap* between the laboratory demonstrations and a practical e-nose microdevice suitable for up-to-date large-scale microfabrication and capable of operating in real-world

* Corresponding authors. E-mail: vsysoev@sstu.ru (V.V.S.); Achim.Goschnick@imt.fzk.de (J.G.); akolmakov@physics.siu.edu (A.K.).
† Saratov State Technical University.
‡ Forschungszentrum Karlsruhe.
§ Southern Illinois University.

10.1021/nl071815+ CCC: $37.00
Published on Web 10/10/2007

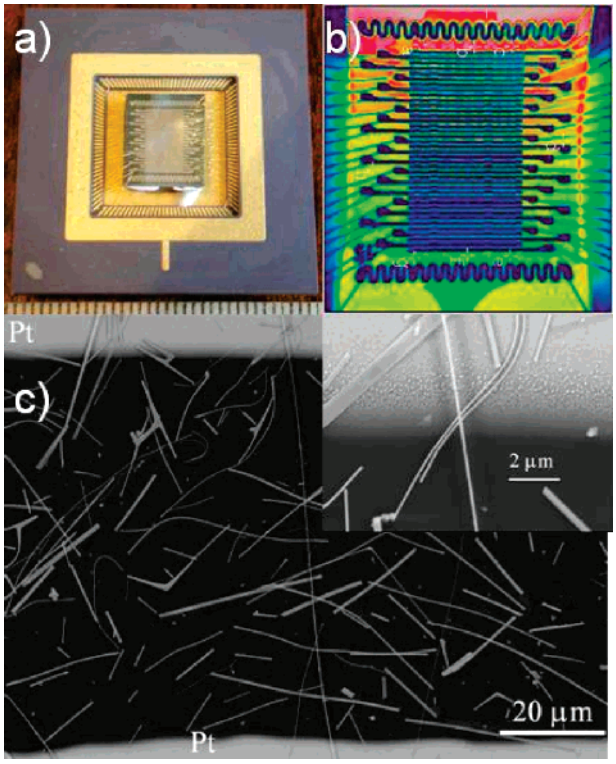

Figure 1. (a) KAMINA microarray chip with SnO_2 nanowire sensing elements; (b) IR image of the chip under application of temperature gradient, 520 K (green area) - 600 K (red area) along the electrode array; (c) SEM image of SnO_2 nanowires on SiO_2/Si/SiO_2 substrate between two Pt complanar electrode strips.

environments. Hence, our aim was to bridge this gap and demonstrate the excellent performance of a practical device made by combining "bottom-up" fabricated SnO_2 nanowires/nanobelts as sensing elements with a "top-down" technology of the state-of-the-art multielectrode KAMINA platform[33,34] (Figure 1a,b).

The key feature of the innovative KAMINA technology is the substitution of an ensemble of separate conventional sensors with the *gradient technique* applied to a single metal oxide layer. The latter is usually deposited onto an array of Pt strips to form a multitude of sensor segments between them (Figure 1b). To differentiate the response of sensor elements, *two gradients* are usually applied across the microarray: (i) the lateral variation of the surface temperature of the film and (ii) the gradual thickness change of the gas-permeable coating topping the metal oxide layer (the latter was not applied so far with the nanowire layers). In this report, we demonstrate that already the nanowire density variation over the segments alone can provide substantial differences in the conductivity patterns of the gradient microarray and establishes a gas discriminating action of the array. When an additional temperature gradient is applied, it reinforces the discrimination power. Hence, we show that new nanowire-based sensing elements with their density variation coupled with a temperature gradient lead to a new discrimination mechanism in multielectrode e-noses.

The SnO_2 nanowires were synthesized at 1280 K under ca. 200 Torr of Ar carrier gas according to previously reported protocols.[32] Briefly, the nanowires (and coproduct nanobelts) were grown on alumina plates and dry-pressed mechanically onto the 4 × 8 mm^2 area of the KAMINA's SiO_2/Si/SiO_2 substrate[34] foreseen to carry the metal oxide gas detection layer and equipped with predeposited coplanar 39 Pt electrodes (see Figure 1c and Section 1 in Supporting Information). The electrodes, 1 μm thick, were fabricated by rf magnetron sputtering through a shadow mask. To preserve the surface of the nanowires from contamination, no wet processes (such as those used in resist-based lithography) were employed at any stage of the chip fabrication or characterization. To create the desired temperature profile across the array of gas-sensing segments, each substrate rear side was equipped with four meander-shaped Pt heaters. The adhesion of the nanofibers to the wafer and to the electrodes was found to be excellent, presumably due to the electrostatic affinity of the SiO_2 surface. The morphology of the nanowire layers was inspected with a scanning electron microscope (SEM). Figure 1c shows the SEM image of the chip surface used in this study. As can be seen, the average sensing element contains a low-density layer of percolating nanowires and nanobelts with characteristic diameters in the range of 50−500 nm and a length from a few up to hundred micrometers. Some of the nanofibers are long enough to bridge the 70 μm gap between the electrodes, while most others form percolating networks.

The X-ray diffraction (XRD) pattern of the nanowire layer, deposited on a SiO_2/Si wafer, is shown in Figure 2a. The major observed reflexes correspond to a SnO_2 rutile single crystal with no other phases present, thus revealing the structural and chemical homogeneity of the nanowire samples. X-ray photoelectron spectroscopy (XPS) spectra taken from as-prepared nanowire layers (Figure 2b) under ultrahigh vacuum conditions (see Section 1 in Supporting Information) confirms the generic purity of the obtained nanowire deposits and qualitatively defines the degree of oxygen deficiency in the topmost surface layers of these nearly stoichiometric SnO_2 nanowires (see discussion below).

To carry out conductometric gas-sensing tests, the coated chips were mounted and wire-bonded into pin−grid−array (PGA) carriers (see Figure 1a) compatible with KAMINA's standard chip housing to provide controlled fluidics for the analyte gas. The housed chips were exposed to pulses of three model gases diluted to a variety of concentrations in dry synthetic air: 2-propanol (0.5−50 ppm), ethanol (0.5−50 ppm), and CO (0.5−10 ppm). Test gas and clean air pulses were periodically alternated at a flow rate of 0.33 L/min. The electrical resistances of the nanowire segments were recorded with a rate of 0.3 Hz for the readout of the entire microarray by the PC-controlled KAMINA electronics. The values measured were in the range of 0.1−20 MΩ. The gas response from the nanowire array was investigated while operating the chip under two different thermal regimes: (i) quasihomogeneous temperature distribution (isothermal) (ca. 580 ± 10 K) and (ii) applying a spatial temperature gradient of 520−600 K across the chip. The surface temperature was monitored and controlled through two Pt meander thermoresistors placed aside the nanowire layer and visualized using an IR camera (Figure 1b).

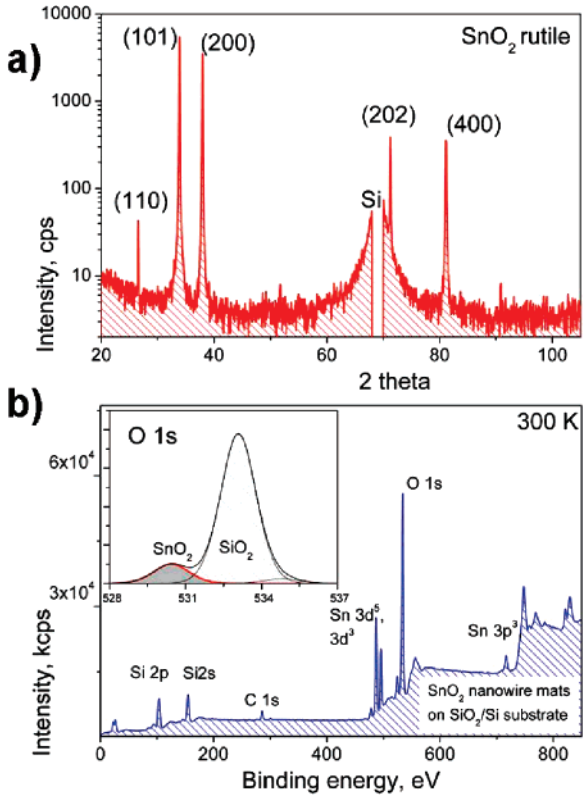

Figure 2. (a) XRD (log scale) and (b) XPS spectra taken from SnO_2 nanowire layer dispersed on the SiO_2/Si wafer demonstrate the structural homogeneity (rutile) and surface purity of the prepared nanowire sensing elements. Because of preferable growth direction of the nanowires and nanobelts, the intensity of XRD reflexes from (101), (200), (202), and (400) lattice planes exceeds that of (110), which is usually a dominant peak in the spectrum of rutile SnO_2 powder.

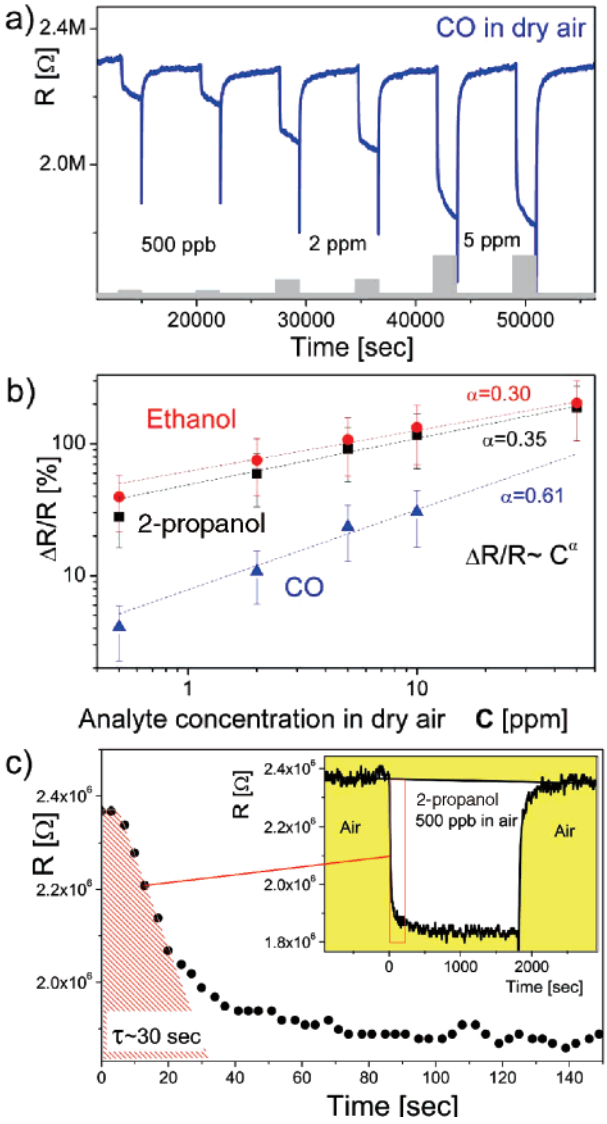

Figure 3. Gas response of the gradient microarray: (a) the median of the nanowire layer resistances during the exposure to a sequence of CO pulses (500 ppb, 2 and 5 ppm); (b) average relative resistance change of the nanowire-equipped segments vs the concentration of the three model gases; all curves follow a power law with the exponent $\alpha = 0.3$ up to 0.6; (c) temporal evolution of the resistance of the middle e-nose segment upon exposure to 500 ppb of 2-propanol in air. The time constant is defined as intersection of the initial slope of the response with its saturated value.

Figure 3a shows the typical isothermal response of the nanowire layer resistance being exposed at 580 K to a pulse sequence of 500 ppb, 2 and 5 ppm of CO. The signal-to-noise ratio obtained from the SnO_2 nanowire mats is excellent. The very similar response to two sequential gas pulses of the same concentration shows the high reproducibility of the nanowire response. Moreover, the magnitude of resistance change under CO exposure is, to our knowledge, comparable to or even better than the best reported results in the literature for undoped SnO_2 in dry air.[35,36] In fact, defining the significance level as three times of the current noise, the detection limit of the nanowire mats for CO is in the range of 150−200 ppb (Figure 3a).

The apparent response time for reducing analytes (elapsed time after exposure to analyte gas), evaluated via analysis of the initial slope of the response (see details in the Figure 3c), was found to be on the order of 30 s, which implies that sensor response time is less than 30 s because the apparent value is convoluted with the contribution from our gas-mixing/delivery setup.

As in the case of the macroscopic oxide surfaces, the oxygen vacancies control the steady state n-type conductance and the surface reactivity of SnO_2 nanowires. Indeed, from XPS characterization of the nanowire mats taken in a wide temperature range, from room temperature up to 570 K (Figure 2b and Supporting Information), we found the nanowire surface stoichiometry (i.e., $x = [O]/[Sn]$ ratio, determined using Sn 3d5/2 (binding energy: 486.4 eV) versus O 1s (530.4 eV) peak's intensity) to be in the vicinity of 1.9. Consistent with other XPS studies taken on SnO_2 polycrystalline films[37,38] and nanofibers,[39] our data thus indicate an oxygen deficiency at the surface of the as-prepared nanowires. Moreover, a decrease in the oxygen content by about 8% was found during annealing of the nanowires at 570 K in vacuum, which can be assigned to thermally induced surface reduction and corroborates the previous UHV studies (see recent comprehensive review ref 40 and references therein). In air, the aforementioned surface vacancies are repopulated back, resulting in ionosorbed

surface oxygen of the general form $O_{\beta S}^{-\alpha}$. The oxygen ionosorption leads to the depletion of the n-type SnO_2 nanowires with electrons in accordance to the surface reaction:[41] $(\beta)/(2)O_2^{gas} + \alpha \cdot e^- + N_S \leftrightarrow O_{\beta S}^{-\alpha}$ (here $\alpha,\beta = \{1,2\}$ accounts for the charge and molecular versus atomic nature of the chemisorbed oxygen and N_S is the concentration of the surface vacancies). Upon adsorbing a reducing gas X, the following surface reaction takes place with the ionosorbed oxygen $\beta \cdot X^{gas} + O_{\beta S}^{-\alpha} \rightarrow \beta \cdot XO^{gas} + \alpha \cdot e^-$, resulting in the donation of electrons back to SnO_2 nanowire.

Figure 3b depicts the dependence of the isothermal relative resistance change $\Delta R/R = (R_{air} - R_{gas})/R_{air}$ of the nanowire layer (averaged over the segments) as a function of the reducing gas concentration C. In accordance with previous results for compact metal oxide surfaces, the $\Delta R/R(C)$ curve obeys a power law with an exponent equal to 0.61 ± 0.06, 0.35 ± 0.03, and 0.30 ± 0.04 for CO, 2-propanol, and ethanol, respectively, which is consistent with Freundlich's adsorption isotherm. Thus, the surface chemistry for SnO_2 nanowire mats so far agrees well with data reported for thin- and thick-film SnO_2 samples.[41,42] Hence, the receptor scheme at this size domain seems to be independent from the morphology of the oxide-sensing element and appears to be governed only by the gas and the doping level the metal oxide. The extrapolation of the straight lines to $\Delta R/R \sim 3\%$ ($\Delta R/R \sim 3\%$ is another alternative way to define the significance level for the signals)[43] indicates CO to be clearly detectable already at less than 500 ppb level, while the alcohols are measurable even at low ppb concentrations.

Although, as can be seen from the above discussion, the general chemical processes (receptor function) are not much affected by the quasi-1D nature of the oxide gas-sensing element, such a high detection power suggests a significant contribution of the nanowire layer morphology to the signal transduction mechanism. Apparently, the current transport via the nanowire mats has a percolating character where the conductance between two adjacent electrodes is determined by the availability of the conduction path(s) through the overlapping single-crystal nanowires (or nanobelts) (Figure 4b). Although the electron transport through such a percolating network can so far only be solved numerically,[44] the major features observed in the sensing performance of the array may be explained qualitatively with a simple core–shell model (see schematics in Figure 4a). Applying the latter to the percolating nanowire layer, we propose that at least two mechanisms contribute concomitantly in the transduction function of the sensors:

(i) Adsorbate-induced change of the potential barrier heights ΔV_S at the contact points between nanowires (see "node" area in the Figure 4a) effectively modulates the transport properties between two overlapping nanowires. Similar to the well-known theory of intergranular contacts,[45,46] the current has to pass at overlapping wires through the charge carrier depletion zones of both wires. Direct imaging of the electrostatic action of such a node was reported in ref 47. The electron transport in the node area can be described in terms of a thermoelectronic emission mechanism (see as an example ref 41) so that the sensor

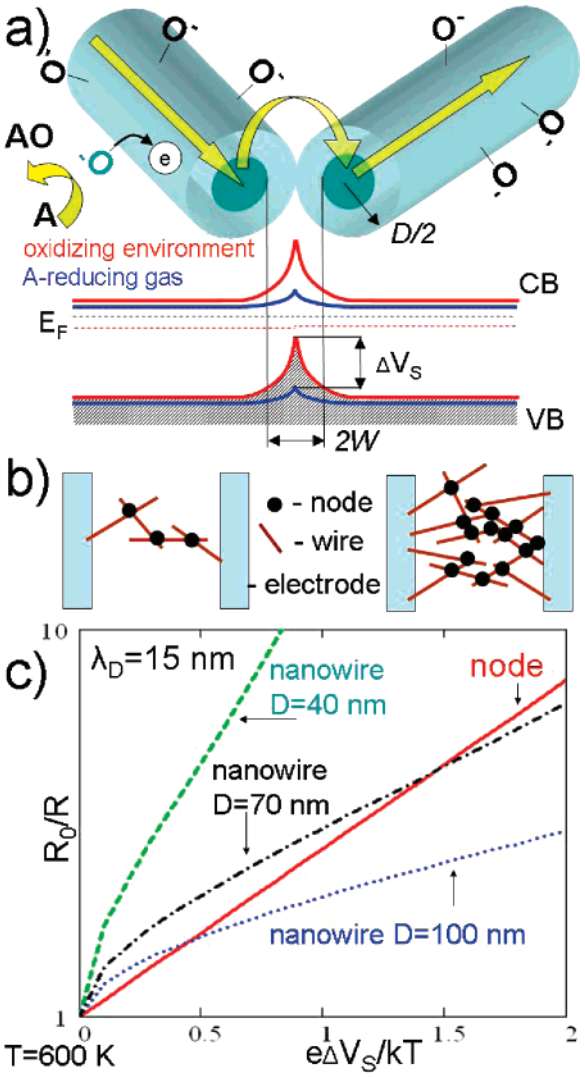

Figure 4. (a) Receptor and transduction functions of the percolating nanowire net. In the oxidizing ambient, the exposure to reducing gas leads to decrease the contact barriers and increase of the cross section of the conducting channels inside the nanowires. (b) Increase of the density of the nanowires leads to an increase of the relative contribution of nodes with respect to straight parts of the percolating path. (c) Comparison of the relative contribution of nodes and nanowires to the sensor signal (log scale).

response due to adsorbate-induced alternating barrier on the node will be:

$$\left.\frac{R_0}{R}\right|_{NODE} \approx \exp\left(\frac{e\Delta V_S}{kT}\right) \quad (1)$$

where R_0 and R are sensor's resistance in air and upon admission of an electron-spending gas, correspondingly, T is the operating temperature, e the elementary charge, and k the Boltzmann's constant.

(ii) Adsorbate influence on the electron transport inside the straight n-type SnO_2 nanowire with diameters of the order of 100 nm exposed to ambient air may be considered within the frame of the simplistic coaxial picture where the semiconducting core of the nanowire is surrounded by an electron depletion region with the width W. The depletion

width depends on the Debye length λ_D of the SnO_2 nanowire ($\lambda_D \sim 10-20$ nm for our moderately doped nanowires)[32,41] and the steady-state coverage of the ionosorbed acceptor molecules (O_2^-, O^-, OH^-) from the ambient at the particular temperature. The depletion width W will change due to a reaction with a reducing gas according to $\Delta W \sim \lambda_D(e\Delta V_S/kT)^{1/2}$, thus "widening" the cross section of the conducting channel. Because of this pure geometrical factor, the sensor signal for the straight nanowire can be estimated as:

$$\left.\frac{R_0}{R}\right|_{WIRE} = \left(\frac{D}{D-2\Delta W}\right)^2 = D^2\left(D - 2\lambda_D\left(\frac{e\Delta V_S}{kT}\right)^{1/2}\right)^{-2} \quad (2)$$

where D is the nanowire diameter.

The relative contributions of these two mechanisms to chemiresistive response are depicted in the Figure 4c. As one can see, for realistic values of $e\Delta V_S/kT \approx 1$ and average diameters of the nanowires to be of 70−100 nm, the resistance ratio of the nodes is comparable to that of the straight parts of the percolating channels. However, because the majority of the nanowires are not long enough to make a direct contact between the electrodes, the electrical current has to flow through node areas. The shorter the wires and the higher the density of statistically distributed wires, the more nodes the current has to pass and the shorter the average travel length between two nodes. This conclusion has important consequences for the discriminating function of the electronic nose and will be discussed below.

As once mentioned, the principle of conventional KAMINA e-nose technology is based on the temperature gradient and a thickness gradient of a gas-permeable metal oxide coating (membrane) established along the array to differentiate the responses from laterally distributed nearly identical individual sensing elements. Because the gas diffusion through the membrane and the redox interactions between analyte molecules and the metal oxide interface are temperature dependent, gas-specific conductivity patterns are usually produced.[48] The performance of the KAMINA array equipped with SnO_2 nanowire mats operated under a temperature gradient is shown in the Figure 5 for 2-propanol as a test gas. As can be seen, at approximately 600 K, the nanowire sensing element reliably and reproducibly responds to as low as 500 ppb of 2-propanol in air which was the lowest concentration used in this study.

Similar response data from all 38 channels are collected, stored, and processed continuously by software to create the "images" of the analyte in the "conductivity patterns" depending on the type of the analyte and its concentration. To test the discrimination power of these conductivity patterns quantitatively, a linear discriminant analysis (LDA)[48−51] was applied. This supervised multivariate pattern recognition method transfers sensor signals (points in the original space of 38 sensor signals) into an optimized coordinate system of lower dimensionality equal to the number of training gases minus one.[50] As the result of the gas specificity of the conductivity patterns, the sensor array response to one gas is distanced from that of another gas in such a coordinate system.[50,51] Apparently, the more different

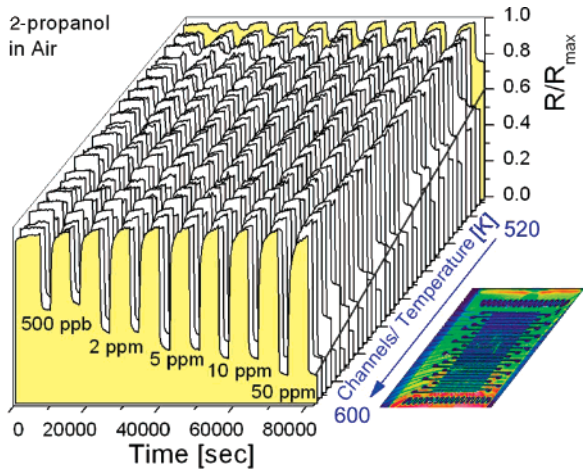

Figure 5. Normalized resistance response of the 38 individual nanowire sensing elements toward 2-propanol pulses when 80 K thermal variation is established along the sensing array. The side line indicates the growth of responsiveness with the temperature.

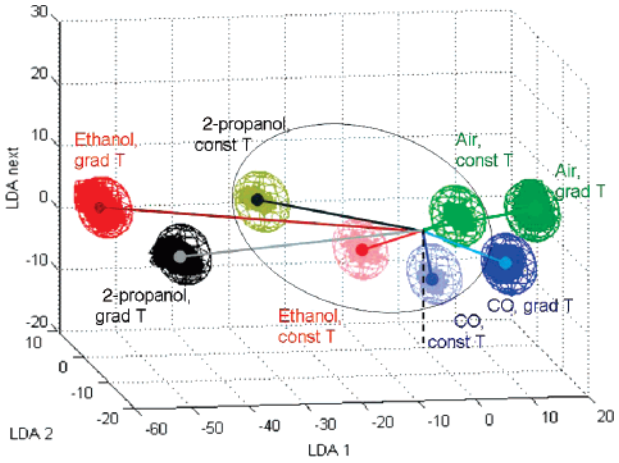

Figure 6. LDA analysis of the conductivity patterns obtained with SnO_2 nanowire-based gradient microarray at exposure to the sample gases (2−10 ppm concentration range). The classification spheres correspond to normal distribution of data at 0.9999 confidence level. The microarray operates under (a) quasihomogeneous heating at 580 K (const T areas inside the ellipse with dimmed colors) and (b) temperature gradient at 520−600 K (grad T areas with bright colors).

(separated) the conductivity patterns for the various trained gases, the better the discrimination power of the e-nose. Figure 6 shows the analysis of the patterns obtained with KAMINA equipped with a SnO_2 nanowire layer. The most striking feature is that the patterns of all model gases are clearly separable and hence can be used to distinguish them. Two very important features can be extracted from this LDA:

(i) The isothermal (taken without thermal gradient) conductivity patterns of the nanowire sensor array are already sufficient to obtain substantially different signal patterns for the various gases (see shadowed central area in the Figure 6). In this case, the average Mahalanobis distance, employed as a quantitative measure to distinguish classes (in our case, the gases) in the LDA, is about 15.3. This means that using nanowire mats as sensing elements in the multielectrode array does not necessarily require the presence of the temperature

gradient. As the microscopic analysis shows, the density of the nanowire layer is stochastically different from segment to segment due to the imponderables of the nanofiber deposition. Therefore, the statistical variations of the nanowires density between electrode arrays alternate the ratio between nodes and nanowire straight segments, thus providing the specificity of the gas response for any individual sensing element. This specificity is particularly crucial for the nanowire densities close to the percolation threshold (Figure 1c) $\rho \sim \langle L_{NW} \rangle^{-2} \sim 2 \times 10^{-3}\ \mu m^{-2}$ (where L_{NW} is an average length of the nanowire).[44] As one can see from the Figure 4b,c, the increase of the density of the nanowires leads to an enhancement of the node contribution in the sensing response. Therefore, the obtained individuality in the response of a specific nanowire sensing segment stems from the unique ratio between the abundances of nodes versus straight parts of the nanowires. Consequently, a gradient or random variations in the nanofiber density can be used, as well as the other gradients such as temperature, nanowire thickness, and surface functionalization, to differentiate the sensor properties of the nanowire gradient microarray.

(ii) If a temperature gradient along the microarray is additionally applied, the discrimination power is significantly enhanced, yielding an average Mahalanobis distance more than twice as large in comparison with the isothermal case (increase from 15.3 to 34.2). Centers of clusters related to gases are "moving away" from the LDA coordinate center, allowing even better recognition of the gas-specific classes. Even the chemically akin alcohols can be distinguished by their conductivity pattern. The additional temperature gradient improves the gas discrimination based on the density differences of the nanowires because of the temperature dependence of the surface chemistry and charge transport of two major partitions (nodes and straight segments) of the percolating network.

In conclusion, the first implementation of SnO_2 nanowires as sensing elements in an electronic micronose based on a gradient gas sensor microarray has been successfully accomplished. The difference in the morphology of these new sensing elements implies a few advantages with respect to traditional ones, namely: (i) High gas permeability is inherent for nanowire mats and does not drop with reduction of the nanowire diameter, as it is a case for nanostructured films. This decoupling of gas permeability and the size of the building block of the sensing element is principal to improve the temporal characteristics of the e-nose. (ii) Nanowire mats possess a dual (nodes versus straight parts of the nanowires) signal transduction mechanism, which is also depend on the percolation regime. The latter opens new opportunities to tune rationally the sensitivity and discrimination power of the electronic nose. (iii) Finally, the single crystallinity of the nanowire building block is going to reduce (and probably eliminate) the aging effects, which are a common drawback for ultrasensitive particulate thin films. These advantageous trends are supported by this research where very high gas sensitivity of the metal oxide nanowire sensing elements is complemented by their fast response time. In fact, to our knowledge, these percolating nanowire sensing elements demonstrate one of the best reported sensitivities with pristine (undoped) SnO_2 sensors to carbon monoxide in air. The excellent discrimination power of such gradient gas sensor microarrays apparently stems out of two cumulative contributions, the spatial temperature gradient and (stochastic) nanowire density difference between the individual sensing elements. The latter alone has been found to be sufficient for isothermal gas discrimination between 2-propanol, ethanol, and CO analytes in air. The comparative studies of the aging effects of nanowire mats and thin films are currently in progress, and preliminary results demonstrate the elevated stability of the nanowire mat sensing elements. Overall, gradient microarrays with sensing elements based on metal oxide nanowire mats of different density appear to be a novel technologically simple and powerful approach for fabrication of the robust, cost-effective, sensitive, and highly selective nose-like gas analytical devices.

Acknowledgment. We thank Dr. D. Fuchs, V. Trouillet, and W. Habicht for XRD, XPS, and SEM measurements, respectively, and Dr. I. Kiselev for development of the software. V.S. thanks DAAD and the Russian Ministry for Education & Science for "Michail Lomonosov" scholarship, no. A/05/58552, and INTAS grant, no. 06-1000014-5877, to support his placements in Germany. At SIUC, part of the research was supported through CATERPILLAR and partially through ACS PRF-G research grants.

Supporting Information Available: Details on the fabrication and characterization of the nanowire sensing elements; general description of the KAMINA unit; procedure of gas response measurements; data processing of the microarray response and applied pattern recognition technique. This material is available free of charge via the Internet at http://pubs.acs.org.

References

(1) Janata, J.; Josowicz, M.; Vanysek, P.; DeVaney, D. M. *Anal. Chem.* **1998**, *70*, 179R.
(2) Buck, L.; Axel, R. *Cell* **1991**, *65*, 175.
(3) Shepherd, G. M. *Nature* **2006**, *444*, 316.
(4) Persaud, K.; Dodd, G. *Nature* **1982**, *299*, 352.
(5) Lundstrom, I.; Erlandsson, R.; Frykman, U.; Hedborg, E.; Spetz, A.; Sundgren, H.; Welin, S.; Winquist, F. *Nature* **1991**, *352*, 47.
(6) Freund, M. S.; Lewis, N. S. *Proc. Natl. Acad. Sci. U.S.A.* **1995**, *92*, 2652.
(7) D'Amico, A.; DiNatale, C.; Paolesse, R. *Sens. Actuators, B* **2000**, *68*, 324.
(8) *Handbook of Machine Olfaction: Electronic Nose Technology*; Pearce, T. C., Schiffman, S. S., Nagle, H. T., Gardner, J. W., Eds.; Wiley-VCH: Weinheim, 2003.
(9) Mitrovics, J.; Ulmer, H.; Weimar, U.; Goepel, W. *Acc. Chem. Res.* **1998**, *31*, 307.
(10) Hagleitner, C.; Hierlemann, A.; Lauge, D.; Kimmer, A.; Kerness, N.; Brand, O.; Baltes, H. *Nature* **2001**, *414*, 293.
(11) Kong, J.; Franklin, N. R.; Zhou, C. W.; Chapline, M. G.; Peng, S.; Cho, K. J.; Dai, H. J. *Science* **2000**, *287*, 622.
(12) Cui, Y.; Wie, Q. Q.; Park, H. K.; Lieber, C. M. *Science* **2001**, *293*, 1289.
(13) Rothschild, A.; Tuller, H. L. *J. Electroceram.* **2006**, *17*, 1005.
(14) Pan, Z. W.; Dai, Z. R.; Wang, Z. L. *Science* **2001**, *291*, 1947.
(15) Huang, M. H.; Wu, Y. Y.; Feick, H.; Tran, N.; Weber, E.; Yang, P. D. *Adv. Mater.* **2001**, *13*, 113.
(16) Liang, C. H.; Meng, G. W.; Wang, G. Z.; Wang, Y. W.; Zhang, L. D.; Zhang, S. Y. *Appl. Phys. Lett.* **2001**, *78*, 3202.
(17) Law, M.; Kind, H.; Messer, B.; Kim, F.; Yang, P. D. *Angew. Chem., Int. Ed.* **2002**, *41*, 2405.

(18) Comini, E.; Faglia, G.; Sberveglieri, G.; Pan, Z. W.; Wang, Z. L. *Appl. Phys. Lett.* **2002**, *81*, 1869.
(19) Arnold, M. S.; Avouris, P.; Pan, Z. W.; Wang, Z. L. *J. Phys. Chem. B* **2003**, *107*, 659.
(20) Li, C.; Zhang, D. H.; Liu, X. L.; Han, S.; Tang, T.; Han, J.; Zhou, C. W. *Appl. Phys. Lett.* **2003**, *82*, 1613.
(21) Kolmakov, A.; Zhang, Y. X.; Cheng, G. S.; Moskovits, M. *Adv. Mater.* **2003**, *15*, 997.
(22) Jiang, X. C.; Wang, Y. L.; Herricks, T.; Xia, Y. N. *J. Mater. Chem.* **2004**, *14*, 695.
(23) Fan, Z. Y.; Wang, D. W.; Chang, P. C.; Tseng, W. Y.; Lu, J. G. *Appl. Phys. Lett.* **2004**, *85*, 5923.
(24) Wang, H. T.; Kang, B. S.; Ren, F.; Tien, L. C.; Sadik, P. W.; Norton, D. P.; Pearton, S. J.; Lin, J. *Appl. Phys. Lett.* **2005**, *86*, 243503.
(25) Ponzoni, A.; Comini, E.; Sberveglieri, G.; Zhou, J.; Deng, S. Z.; Xu, N. S.; Ding, Y.; Wang, Z. L. *Appl. Phys. Lett.* **2006**, *88*, 203101.
(26) Madou, M. J.; Morrison, S. R. *Chemical Sensing with Solid State Devices*; Academic Press: San Diego, 1989.
(27) Lilach, Y.; Zhang, J.-P.; Moskovits, M.; Kolmakov, A. *Nano Lett.* **2005**, *5*, 2019.
(28) Dmitriev, S.; Lilach, Y.; Button, B.; Moskovits, M.; Kolmakov, A. *Nanotechnology* **2007**, *18*, 055707.
(29) Kolmakov, A. *Proc. SPIE* **2006**, *6370*, 63700X.
(30) Kolmakov, A.; Moskovits, M. *Annu. Rev. Mater. Res.* **2004**, *34*, 151.
(31) Comini, E. *Anal. Chim. Acta* **2006**, *568*, 28.
(32) Sysoev, V. V.; Button, B. K.; Wepsiec, K.; Dmitriev, S.; Kolmakov, A. *Nano Lett.* **2006**, *6*, 1584.
(33) KArlsruhe Micro NAse.
(34) Goschnick, J. *Microelectron. Eng.* **2001**, *57*−*58*, 693.
(35) Dolbec, R.; El Khakani, M. A. *Appl. Phys. Lett.* **2007**, *90*, 173114.
(36) Hernández-Ramírez, F.; Tarancón, A.; Casals, O.; Arbiol, J.; Romano-Rodríquez, A.; Morante, J. R. *Sens., Actuators B* **2007**, *121*, 3.
(37) Sinner-Hettenbach, M.; Göthelid, M.; Weissenrieder, J.; von Schenck, H.; Weiss, T.; Barsan, N.; Weimar, U. *Surf. Sci.* **2001**, *477*, 50−58.
(38) Moroseac, M.; Skála, T.; Veltruská, K.; Matolín, V.; Matolínová, I. *Surf. Sci.* **2004**, *566*, 1118−1123.
(39) Wang, Y.; Aponte, M.; Leon, N.; Ramos, I.; Furlan, R.; Pinto, N.; Evoy, S.; Santiago-Aviles, J. J. *J. Am. Ceram. Soc.* **2005**, *88*, 2059−2063.
(40) Batzill, M., Diebold, U. *Prog. Surf. Sci.* **2005**, *79* (2−4), 47−154
(41) Barsan, N.; Weimar, U. *J. Electroceram.* **2001**, *7*, 143−167.
(42) *Semiconductor Sensors in Physicochemical Studies*; Kupriyanov, L. Yu., Ed.; Elsevier: Amsterdam, 1996.
(43) *Sensors: A Comprehensive Survey, Vol. 1: Fundamentals and General Aspects*; Goepel, W., Hesse, J., Zemel, J. N., Eds.; VCH: Weinheim, 1989. Also, D'Amico, A.; Di Natale, C. *IEEE Sens. J.* **2001**, *1*, 183−190.
(44) Kumar, S.; Murthy, J. Y.; Alam, M. A. *Phys. Rev. Lett.* **2005**, *95*, 066802.
(45) Stauffer, D.; Aharony, A. *Introduction to Percolation Theory*, 2nd ed.; Taylor & Francis: London, 1992.
(46) Sukharev, V. Ya. *J. Chem. Soc., Faraday Trans.* **1993**, *89*, 559−572.
(47) Kalinin, S. V.; Shin, J.; Jesse, S.; Geohegan, D.; Baddorf, A. P.; Lilach, Y.; Moskovits, M.; Kolmakov, A. *J. Appl. Phys.* **2005**, *98*, 044503.
(48) Sysoev, V. V.; Kiselev, I.; Frietsch, M.; Goschnick, J. *Sensors* **2004**, *4*, 37.
(49) Henrion, R.; Henrion, G. *Multivariate Datenanalyse*; Springer-Verlag: Berlin, 1995.
(50) Jurs, P. C.; Bakken, G. A.; McClelland, H. E. *Chem. Rev.* **2000**, *100*, 2649.
(51) Albert, K. J.; Lewis, N. S.; Schauer, C. L.; Sotzing, G. A.; Stitzel, S. E.; Vaid, T. P.; Walt, D. R. *Chem. Rev.* **2000**, *100*, 2595.

NL071815+